Atmospheric
Chemistry
and Physics
Discussions

Open Access

EGU

How alkaline compounds control atmospheric aerosol acidity

Vlassis A. Karydis[1,2*], Alexandra P. Tsimpidi[1,2,3], Andrea Pozzer[1,4], and Jos Lelieveld[1,5]

[1] Max Planck Institute for Chemistry, Atmospheric Chemistry Dept., Mainz, 55128, Germany.

5 [2] Now at Forschungszentrum Jülich, Inst. for Energy and Climate Research, IEK-8, Jülich, 52425, Germany.

[3] National Observatory of Athens, Inst. for Environmental Research and Sustainable Development, Athens, 15236, Greece.

[4] International Centre for Theoretical Physics, Trieste, 34151, Italy

[5] The Cyprus Institute, Climate and Atmosphere Research Center Nicosia, 1645, Cyprus.

10 *Correspondence to*: Vlassis A. Karydis (v.karydis@fz-juelich.de)

Abstract. The acidity of atmospheric aerosols regulates the particulate mass, composition and toxicity, and has important consequences for public health, ecosystems and climate. Despite these broad impacts, the global distribution and evolution of aerosol acidity are unknown. We used the particular, comprehensive atmospheric multiphase chemistry – climate model EMAC to investigate the main factors that control aerosol acidity, and uncovered remarkable variability and unexpected

15 trends during the past 50 years in different parts of the world. We find that alkaline compounds, notably ammonium, and to a lesser extent crustal cations, buffer the aerosol pH on a global scale. Given the importance of aerosols for the atmospheric energy budget, cloud formation, pollutant deposition and public health, alkaline species hold the key to control strategies for air quality and climate change.

1. Introduction

20 Aerosol acidity is a central property of atmospheric particulates that influence clouds, climate and air quality, including impacts on human health (Raizenne et al., 1996;Lelieveld et al., 2015). It affects the partitioning of semi-volatile acids between the gas and aerosol phases (Guo et al., 2016;Guo et al., 2017;Guo et al., 2018;Nenes et al., 2020), secondary organic aerosol (SOA) formation (Xu et al., 2015;Marais et al., 2016), the solubility of trace metals in aerosols (Oakes et al., 2012), associated with their toxicity (Fang et al., 2017) and nutrient capacity (Jickells et al., 2005), the activation of halogens that

25 act as oxidants (Saiz-Lopez and von Glasow, 2012), the conversion of sulfur dioxide (Seinfeld and Pandis, 2006;Cheng et al., 2016), the particle hygroscopic growth and lifetime (Metzger et al., 2006;Abdelkader et al., 2015;Karydis et al., 2016), and atmospheric corrosivity (Leygraf et al., 2016). Direct measurement of aerosol acidity is difficult and associated with much uncertainty, being dependent on filter sampling and the H^+ molality in the aqueous extract, which is sensitive to artifacts (Pathak et al., 2004). Therefore, particle pH, a commonly used acidity metric of aqueous aerosols, is typically

30   inferred by proxy techniques (Hennigan et al., 2015;Pye et al., 2020). Two of the most common are the ion balance and the
molar ratio methods. In the past, these methods did not consider the effects of aerosol water and multiphase interactions with
gas phase species (Hennigan et al., 2015). The simultaneous measurement of gas phase species can improve aerosol pH
estimates by accounting for the phase partitioning of semi-volatile species (e.g., NH_3, HNO_3). However, the accuracy of this
approach relies on the availability of information on these species in both the gas and aerosol phase, being scant in most
35   cases.

The best estimates of pH are obtained with thermodynamic equilibrium models, although the accuracy can be limited by not
accounting for all ionic species. For example, most atmospheric chemistry models do not consider crustal elements (e.g.,
Ca^{2+}, Mg^{2+}, K^+). These species affect the ion balance by influencing the phase partitioning of nitrate and ammonium,
especially in areas where aeolian dust is abundant (Karydis et al., 2016). Here we present 50-year global acidity trends of
40   fine aerosols (i.e. with a diameter < 2.5 μm) by employing the EMAC chemistry – climate model (Jöckel et al., 2010). The
pH calculations are performed online with the ISORROPIA II thermodynamic equilibrium model (Fountoukis and Nenes,
2007).

2. Results and Discussion

2.1 Global variability of aerosol acidity

45   Figure 1 shows the modeled near-surface distribution of fine aerosol acidity for the 2010-2015 period. We find
predominantly acidic particles over the anthropogenically influenced regions in the northern hemisphere and the tropical
biomass burning zones, and mostly alkaline particles over deserts and oceans, especially over the southern oceans. The pH
typically ranges from 4.0 to 6.7 (5.3 on average) over the western USA since it is affected by crustal cations from the
surrounding deserts. Therefore, the pH calculations in this region are sensitive to the aerosol state assumption. Over
50   Pasadena, the base case model using the stable state mode estimates a mean pH of 5.9 units, while the sensitivity simulation
with only liquid aerosols results in 2.7 pH units (equal to Guo et al. (2017) estimations by using the metastable assumption;
Table S1). Over Europe, the pH ranges from 2.6 to 6.7 (3.9 on average). Observational estimates of aerosol pH from the Po
Valley (Squizzato et al., 2013;Masiol et al., 2020) and Cabauw (Guo et al., 2018) support the relatively low acidity of fine
aerosols over Europe (Table S1). Model calculations compare well with observational estimates from Cabauw, however,
55   result in higher pH (~1 unit) compared to values from Po Valley (estimated by using the E-AIM model). Over East Asia the
average pH is 4.7, ranging from 2.6 to 7.4. Relatively high pH's are found over regions where anthropogenic aerosols are
mixed with aeolian dust, e.g., from the Gobi Desert, which buffer the acidity (e.g., ~6 pH units over Hohhot, which agrees
well with the estimations of Wang et al. (2019a)). The relatively low pH in large parts of Asia is explained by strong SO_2
emissions and associated sulfate, which have increased strongly in the past decades (e.g., over Guangzhou, supported by
60   estimations of Jia et al. (2018)). Estimates of unrealistically high aerosol acidity can result from omitting the gas phase

concentrations of semi-volatile ions from the pH calculations (e.g., estimates over Hong Kong (Yao et al., 2007;Xue et al., 2011), Singapore (Behera et al., 2013) and Shanghai (Pathak et al., 2009); Table S1). At the same time, SO_2 emissions have decreased over Europe and USA, and recently in China. However, aerosols over the eastern USA have remained acidic, with an average pH of 3.0 until recently, corroborating the findings of Weber et al. (2016) and Lawal et al. (2018) that aerosol acidity over this region is less sensitive to SO_2 than to NH_3 emissions.

The aerosol pH over the anthropogenically-influenced northern hemispheric mid-latitudes exhibits a clear seasonal pattern with lower values during boreal summer and higher ones during winter, driven by the availability of ammonium and by the aerosol water content (Fig. 2). This is evident from both our model calculations and from observational estimates mostly in heavily populated areas such as the Po Valley (Squizzato et al., 2013), Beijing (Tan et al., 2018), and Tianjin (Shi et al., 2017), and to a lesser extent over areas strongly affected by aeolian dust (e.g., Hohhot; Wang et al., 2019b) (Table S1). Over tropical regions, fine particulates have a pH between 3.2 and 7.4, being strongly influenced by pyrogenic potassium, i.e., from widespread biomass burning (Metzger et al., 2006), and a high aerosol water content. Observational estimates from Sao Paulo support these high pH values (Vieira-Filho et al., 2016), albeit with 1 unit bias mainly related to the use of the E-AIM model. Over deserts, aerosols are relatively alkaline, with a pH up to 7.4. Aerosols in the marine environment tend to be alkaline also, with a pH up to 7.4 over the southern oceans. Observational estimates report highly acidic aerosols over the southern oceans due to the lack of gas phase input for the pH calculations (Dall'Osto et al., 2019). Over the Arctic and the northern Atlantic and Pacific Oceans, aerosol acidity is significantly enhanced by strong sulfur emissions from international shipping and pollution transport from industrialized areas. The pH over the northern extratropical oceans and the Arctic ranges from 2.0 to 7.0 with an average of about 5.2. The annual cycle of aerosol acidity over these regions is strongly influenced by anthropogenic pollution, being relatively high during boreal summer. Over the Antarctic, aerosol pH ranges from 4.5 to 7.0 and follows a clear seasonal pattern (Fig. 2).

2.2 Temporal evolution of aerosol acidity

Figure 1 and Table 1 present the aerosol pH over the period 1970-2020. We investigated the impacts of alkaline species by omitting the emissions of ammonia and mineral cations in two sensitivity simulations.

2.2.1 Europe

Over Europe, the pH has increased strongly from about 2.8 during the 1970s to 3.9 recently. Especially during the 1990s NH_3 emissions over Europe increased significantly by 14%, while at the same time NOx and SO_2 emissions decreased by 13% and 49%, respectively. While this trend has continued in the past decade, pH changes slowed because the sulfate and nitrate decreases have been compensated through volatilization of ammonia from the particles. In addition, the recently increasing cation/anion ratio is accompanied by a reduction of aerosol water, preventing a significant decrease of the aerosol acidity (Fig. S1). Overall, the increase of aerosol pH by more than 1 unit during the last 50 years had a significant impact on the gas-particle partitioning of semi-volatile acids, e.g., nitric acid, since their dissociation into ions enhances their solubility

Atmospheric
Chemistry
and Physics
Discussions

(Nah et al., 2018). Here, the fraction of nitrate in the particle phase relative to total nitrate (gas plus particle) has increased from ~70% to 85% (Fig. 3). The increase in aerosol pH has been accompanied by an increase in aerosol hygroscopicity (Fig.

95 4). After the substantial reduction of SO_2 emissions, sulfate salts (e.g., ammonium sulphate) are replaced by more hygroscopic nitrate salts (e.g., ammonium nitrate) in the aerosol composition. In addition, the decrease of organic compound emissions during the last 50 years contributed to the increase of the aerosol hygroscopicity. Our sensitivity simulations reveal that aerosol acidity over Europe is highly sensitive to NH_3 emissions. Despite the decline of both SO_2 and NOx during the past decades, the aerosol would have remained highly acidic (pH ~1) in the absence of NH_3.

100 **2.2.2 North America**

Over North America, aerosol acidity also decreased with SO_2 and NOx emissions. Nevertheless, these emissions are still relatively strong in the eastern USA (5 times higher than in the western USA) resulting in very acidic aerosols, with a pH ranging from 2.2 in 1971 to 3.3 recently (Figs. 1 and S1). Such acidic conditions promote the dissolution of metals (e.g., Fe, Mn, Cu) in ambient particles (Fang et al., 2017). Soluble transition metals in atmospheric aerosols have been linked to

105 adverse health impacts since they generate reactive oxygen species, leading to oxidative stress and increased toxicity of fine particulate matter (Fang et al., 2017;Park et al., 2018). Since the solubility of transition metals increases exponentially below a pH of 3, the decrease of aerosol acidity over the eastern USA reported here suggests that the particles have become substantially less toxic in the past few decades. Similar to Europe, the increasing pH has resulted in a growing aerosol nitrate fraction from ~50% during the 1970s to 65% recently (Fig. 3), and to a strong increase of aerosol hygroscopicity by ~0.15

110 units at the cloud base (Fig. 4). The role of NH_3 is critically important; without it the aerosol pH over the eastern USA would be close to zero. Over the western USA, the aerosol pH is higher (~5), being affected by aeolian dust from the Great Basin Desert, although NH_3 is still the most important alkaline buffer.

2.2.3 East and South Asia

In Asia, SO_2 and NOx emissions have increased drastically since 1970. However, the simultaneous increase of NH_3

115 emissions along with the presence of mineral dust from the surrounding deserts (i.e., Gobi, Taklimakan, Thar) decelerated the increase of aerosol acidity. Over East Asia, the aerosol pH decreased from about 5.3 during the 1970s to 4.5 in 2010. This change in aerosol acidity has affected the predominant pathway of sulfate formation through aqueous phase chemistry. Under acidic conditions, SO_2 is mainly oxidized by dissolved H_2O_2, while at pH > 5 the oxidation by O_3 predominates (Seinfeld and Pandis, 2006). Therefore, the decrease of pH during the last 50 years, even though being relatively modest,

120 was sufficient to turn-off sulfate production from O_3 oxidation (Fig. 5). At the same time, the increased aerosol acidity hinders the partitioning of nitric acid to the aerosol phase, reducing the aerosol nitrate fraction from 90% to 80% (Fig. 3). Remarkably, the aerosol hygroscopicity has increased from ~0.3 in the 1970s to 0.45 recently (Fig. 4), revealing a reverse development compared to Europe and the USA. Here, the fraction of mineral dust in the aerosol is higher; therefore, the particles gained hygroscopicity by the acquired pollution solutes. Recently, the SO_2 emissions have dropped and the NOx

125   emission increase has slowed in East Asia, while SO_2 emissions are soaring in South Asia. SO_2 emission trends since 2007 have been so drastic that inventories and scenarios tend to underestimate them. Satellite observations indicate that India has recently overtaken China as the world largest emitter of SO_2 (Li et al., 2017). Following the satellite observations, we implemented the large SO_2 trends into our model (Fig. S2). Surprisingly, the effect only becomes noticeable over East Asia after 2016, when the aerosol pH started increasing by about 0.3 units, while we do not find any change over South Asia. This

130   corroborates the strong buffering that we found over other regions such as Europe. Fig. 1 shows that NH_3 has been the major buffer, supporting the recent findings of Zheng et al. (2020) that the acid-base pair of NH_4^+/NH_3 provides the largest buffering capacity over East and South Asia. However, we also found that in East Asia and to a lesser extent in South Asia crustal elements, not considered in the study of Zheng et al. (2020), have contributed significantly on maintaining a mean pH of 4.5 – 5 in the past decade (Fig. 1).

2.2.4 Tropical forests, Middle East

Over tropical forests, aerosols are typically not very acidic with pH values >4. Note that organic acids were not included in the aerosol pH calculations, however, their contribution to the total ionic load is small (Andreae et al., 1988;Falkovich et al., 2005), and aerosol acidity can be attributed to inorganic acids. Over the Amazon and Congo basins, the aerosol pH remained around 5 since 1970. The Southeast Asian forest atmosphere is affected by pollution from mainland Asia, and the aerosol pH

140   decreased to around 4 recently. This pH drop has enhanced SOA formation from isoprene, since under low-NOx conditions (typical over rainforests) the presence of acidifying sulfate increases the reactive uptake of epoxydiols (Xu et al., 2015;Surratt et al., 2010). Nevertheless, NH_3 emissions provide a remarkably strong buffer over all three tropical regions while mineral dust cations are also important over the Amazon and Congo forests. Further, the Middle East is affected by strong anthropogenic (fossil fuel related) and natural (aeolian dust) aerosol sources. Due to the high abundance of mineral

145   dust, the pH has remained close to 7. Without crustal cations, the pH would drop to about 4. Despite the omnipresence of alkaline species from the surrounding deserts, NH_3 still plays a central role in controlling the acidification of mineral dust aerosols, which can affect their hygroscopic growth and hence their climate forcing (Klingmuller et al., 2019;Klingmüller et al., 2020).

2.2.5 Oceans

150   Over the Arctic and northern extra-tropical oceans, aerosol acidity is strongly affected by pollution transport from the urban-industrial mid-latitudes. The Arctic aerosol pH is highly variable, remaining relatively low up to 1990 (~4.2), after which it increased to about 5.2. Crustal cations are found to play a significant buffering role. Over the northern extra-tropical oceans, aerosol pH has remained relatively constant (~4.8). NH_3 provides an important alkaline buffer, and without it the aerosol pH would have been below 3. NH_3 also proved to be important over the tropical and southern extra-tropical oceans, where a

155   noticeable increase in aerosol acidity occurred after June 1991, when the eruption of Mount Pinatubo in the Philippines released ~20 million tons of SO_2 into the stratosphere (McCormick et al., 1995). The impact of Pinatubo sulfate, after

returning to the troposphere, on aerosol acidity is mostly evident over Antarctica, where the pH dropped by 2 units, as the stratospheric circulation is strongest in the winter hemisphere. Over Antarctica concentrations of dust and especially of NH_3 are very low, and Fig. 1 illustrates that only in this pristine environment the large Pinatubo anomaly could overwhelm the

160   buffering by alkaline species. Except after Pinatubo, the pH has remained nearly constant at 5.8 over Antarctica and about 5.5 in the tropics and 6.8 in the southern extra-tropics.

3. Conclusions

We find that aerosol pH is generally well-buffered by alkaline compounds, notably NH_3 and in some areas crustal elements. NH_3 is found to supply remarkable buffering capacity on a global scale, from the polluted continents to the remote oceans. In

165   the absence of NH_3, aerosols would be highly (to extremely) acidic in most of the world. Therefore, potential future changes in NH_3 are critically important in this respect. Agriculture is the main NH_3 source and a controlling factor in fine particle concentrations and health impacts in some areas (e.g., Europe) (Pozzer et al., 2017). The control of agricultural ammonia emissions must therefore be accompanied by very strong reductions of SO_2 and NOx to avoid that aerosols become highly acidic with implications for human health (aerosol toxicity), ecosystems (acid deposition and nutrient availability), clouds

170   and climate (aerosol hygroscopicity).

4. Appendix A: Materials and Methods

4.1 Aerosol-chemistry-climate model

We used the ECHAM5/MESSy Atmospheric Chemistry (EMAC) model, which is a numerical chemistry and climate simulation system that describes lower and middle atmosphere processes (Jöckel et al., 2006). EMAC uses the Modular

175   Earth Submodel System (MESSy2) (Jöckel et al., 2010) to link the different sub-models with an atmospheric dynamical core, being an updated version of the 5th generation European Centre - Hamburg general circulation model (ECHAM5) (Roeckner et al., 2006). EMAC has been extensively described and evaluated against in situ observations and satellite retrievals to compute particulate matter concentrations and composition, aerosol optical depth, acid deposition, gas phase mixing ratios, cloud properties, and meteorological parameters (Karydis et al., 2016;Pozzer et al., 2012;Tsimpidi et al., 2016;Karydis et al.,

180   2017;Bacer et al., 2018). The spectral resolution of EMAC used in this study is T63L31, corresponding to a horizontal grid resolution of approximately $1.9^{o}x1.9^{o}$ and 31 vertical layers extending up to 10 hPa (i.e., 25 km) from the surface. The presented model simulations encompass the 50-year period 1970-2020.

EMAC calculates fields of gas phase species online through the Module Efficiently Calculating the Chemistry of the Atmosphere (MECCA) Submodel (Sander et al., 2019). MECCA calculates the concentration of a range of gases, including

185   aerosol precursor species (e.g. SO_2, NH_3, NO_x, DMS, H_2SO_4 and DMSO) and the major oxidant species (e.g. OH, H_2O_2,

Atmospheric
Chemistry
and Physics
Discussions

NO_3, and O_3). Aerosol microphysics are calculated by the Global Modal-aerosol eXtension (GMXe) module (Pringle et al., 2010). The organic aerosol formation and atmospheric evolution are calculated by the ORACLE Submodel (Tsimpidi et al., 2014, 2018). The aerosol size distribution is described by seven lognormal modes: four hydrophilic modes that cover the aerosol size spectrum of nucleation, Aitken, accumulation and coarse modes, and three hydrophobic modes that cover the

190   same size range except nucleation. The aerosol composition within each size mode is uniform (internally mixed), however, it varies between modes (externally mixed). Each mode is defined in terms of total number concentration, number mean radius, and geometric standard deviation (Pringle et al., 2010). The removal of gas and aerosol species through wet and dry deposition is calculated within the SCAV (Tost et al., 2006) and DRYDEP (Kerkweg et al., 2006) submodels, respectively. The sedimentation of aerosols is calculated within the SEDI submodel (Kerkweg et al., 2006). The cloud cover,

195   microphysics and precipitation of large scale clouds is calculated by the CLOUD Submodel (Roeckner et al., 2006) which uses a two-moment stratiform microphysical scheme (Lohmann and Ferrachat, 2010), and describes liquid droplet (Karydis et al., 2017) and ice crystal (Bacer et al., 2018) formation by accounting for the aerosol physicochemical properties. The effective hygroscopicity parameter κ is used to describe the influence of chemical composition on the cloud condensation nuclei (CCN) activity of atmospheric aerosols. κ is calculated using the mixing rule of Petters and Kreidenweis (Petters and

200   Kreidenweis, 2007) and the individual κ parameter values for each inorganic salt (Petters and Kreidenweis, 2007;Sullivan et al., 2009). Organic aerosol species are assumed to have a constant hygroscopicity parameter κ of 0.14 while bulk mineral dust and black carbon are assumed to have zero hygroscopicity.

4.2 Thermodynamic model

The inorganic aerosol composition, which is of prime importance for the accurate pH calculation, is computed with the

205   ISORROPIA-II thermodynamic equilibrium model (Fountoukis and Nenes, 2007). ISORROPIA-II calculates the gas/liquid/solid equilibrium partitioning of the K^+-Ca^{2+}-Mg^{2+}-NH_4^+-Na^+-SO_4^{2-}-NO_3^--Cl^--H_2O aerosol system and considers the presence of 15 aqueous phase components and 19 salts in the solid phase. ISORROPIA-II solves for the equilibrium state by considering the chemical potential of the species and minimizes the number of equations and iterations required by considering specific compositional "regimes". Furthermore, to account for kinetic limitations by mass transfer and transport

210   between the gas and particle phases, the process of gas/aerosol partitioning is calculated in two stages (Pringle et al., 2010). First, the gaseous species that kinetically condense onto the aerosol phase within the model timestep are calculated assuming diffusion limited condensation (Vignati et al., 2004). Then, ISORROPIA-II re-distributes the mass between the gas and the aerosol phase assuming instant equilibrium between the two phases.

ISORROPIA-II is used in the forward mode, in which the total (i.e., gas and aerosol) concentrations are given as input.

215   Reverse mode calculations (i.e. when only the aerosol phase composition is known) should be avoided since they are sensitive to errors and infer bimodal behavior with highly acidic or highly alkaline particles, depending on whether anions or cations are in excess (Song et al., 2018). While it is often assumed that aerosols are in a metastable state (i.e., composed only

Atmospheric
Chemistry
and Physics
Discussions

of a supersaturated aqueous phase), here we use ISORROPIA-II in the thermodynamically stable state mode where salts are allowed to precipitate once the aqueous phase becomes saturated. For this purpose, we have used the revised ISORROPIA-II

220 model which includes modifications proposed by Song et al. (2018), who resolved coding errors related to pH calculations when the stable state assumption is used. A sensitivity simulation with only liquid aerosols (i.e., metastable) revealed that the assumed particle phase state does not significantly impact the pH calculations over oceans and polluted regions (e.g., Europe), however, the metastable assumption produces more acidic particles (up to 2 units of pH) in regions affected by high concentrations of crustal cations (Fig. S3). Overall, the stable state assumption used here produces about 0.5 units higher

225 global average pH than the metastable assumption. By comparing with the benchmark thermodynamic model E-AIM, Song et al. (2018) found that ISORROPIA-II produces somewhat higher pH (by 0.1-0.7 units, negatively correlated with RH). However, E-AIM model versions either lack crustal cations from the ambient mixture of components (e.g. version II) (Clegg et al., 1998), or only include Na^+ with the restriction that it should be used when RH> 60% (e.g. version IV) (Friese and Ebel, 2010).

4.3 pH calculations

The pH is defined as the negative decimal logarithm of the hydrogen ion activity ($a_{H^+} = \gamma x_{H^+}$) in a solution:

$$pH = -\log_{10}\left(\gamma x_{H^+}\right) \qquad (A1)$$

where x_{H^+} is the molality of hydrogen ions in the solution and γ is the ion activity coefficient of hydrogen. Assuming that γ is unity, the aerosol pH can be calculated by using the hydrogen ion concentration in the aqueous aerosol phase calculated by

235 ISORROPIA-II (in mole m^{-3}) and the aerosol water content calculated by GMXe (in mole Kg^{-1}). GMXe assumes that particle modes are internally mixed, and takes into account the contribution of both inorganic and organic (based on the organic hygroscopicity parameter, $\kappa_{org} = 0.14$) species to aerosol water.

   The aerosol pH is calculated online, and output stored every five hours based on instantaneous concentrations of fine aerosol water and hydrogen ions. The average pH values shown in the manuscript are the calculated instantaneous mean pH

240 values. According to the Jensen's inequality (Jensen, 1906), the average of the instantaneous pH values is less than or equal to the pH calculated based on the average of the water and hydrogen ion instantaneous values. We estimate that the average pH calculated based on 5-hourly instantaneous values is approximately 1-3 (~2 globally averaged) units higher than the pH calculated based on the average water and hydrogen ion concentrations. By including online gas-particle partitioning calculations of the NH_3/HNO_3 system in polluted air, as applied here, we find that the aerosol pH is higher by approximately

245 one unit (Guo et al., 2015). Hence by neglecting these aspects the aerosol pH would be low-biased by about 3 points.

   The pH calculated here is compared against pH estimations from field derived $PM_{2.5}$ compositional data around the world compiled by Pye et al. (2020) (Table S1). pH data derived from other aerosol sizes (e.g., PM_1) has been omitted since aerosol acidity can vary significantly with size (Zakoura et al., 2020). It should be emphasized that the comparison presented

in Table S1 aims to corroborate the spatial variability of pH found in this study and not to strictly evaluate the model

250   calculations. Observationally estimated aerosol pH is derived from a variety of methods that can affect the result significantly as discussed above (i.e., the use of E-AIM or ISORROPIA, stable/metastable assumption, forward/reverse mode, and the availability of gas phase NH_3/HNO_3, crustal species, and organic aerosol water observations).

4.4 Emissions

The vertically distributed (Pozzer et al., 2009) CMIP5 RCP8.5 emission inventory (van Vuuren et al., 2011) is used for the

255   anthropogenic and biomass burning emissions during the years 1970-2020. Direct emissions of aerosol components from biofuel and open biomass burning are considered by using scaling factors applied on the emitted black carbon based on the findings of Akagi, et al. (Akagi et al., 2011) (Table S2). Dust emission fluxes and emissions of crustal species (Ca^{2+}, Mg^{2+}, K^+, Na^+) are calculated online as described by Klingmuller, et al. (Klingmuller et al., 2018) and based on the chemical composition of the emitted soil particles in every grid cell (Karydis et al., 2016); Table S3. NO_x produced by lightning is

260   calculated online and distributed vertically based on the parameterization of Grewe, et al. (Grewe et al., 2001). The emissions of NO from soils are calculated online based on the algorithm of Yienger and Levy (Yienger and Levy, 1995). The oceanic DMS emissions are calculated online by the AIRSEA Submodel (Pozzer et al., 2006). The natural emissions of NH_3 are based on the GEIA database (Bouwman et al., 1997). Emissions of sea spray aerosols (assuming a composition suggested by Seinfeld and Pandis (Seinfeld and Pandis, 2006); Table S2) and volcanic degassing emissions of SO_2 are based on the

265   offline emission data set of AEROCOM (Dentener et al., 2006).

4.5 Partitioning of nitric acid between the gas and aerosol phases

The impact of pH on the fraction of nitrate in the particle phase relative to total nitrate (gas plus particle), i.e., $\varepsilon(NO_3^-)$, during the 50 years of simulation in specific regions is calculated as follows (Nah et al., 2018):

$$\varepsilon(NO_3^-) = \frac{H_{HNO_3}^* WRT(0.987 \times 10^{-14})}{\gamma_{NO_3^-}\gamma_{H^+}10^{-pH} + H_{HNO_3}^* WRT(0.987 \times 10^{-14})} \quad (A2)$$

Where $H_{HNO_3}^*$ is the combined molality-based equilibrium constant of HNO_3 dissolution and deprotonation, γ's represent the

270   activity coefficients, W is the aerosol water, R is the gas constant, and T is the ambient temperature.

4.6 Sulfate formation in aqueous aerosols

The sulfate production rate on aqueous aerosols from the heterogeneous oxidation of S(IV) with the dissolved O_3 is given by

$$R_0 = k [O_3] \quad (A3)$$

. The first-order uptake rate, k, from monodisperse aerosols with radius r_a and total aerosol surface A, is calculated following

275   Jacob (Jacob, 2000):

$$k = \left(\frac{r_\alpha}{D_g} + \frac{4}{\upsilon\gamma} \right)^{-1} A \quad (A4)$$

where υ is the mean molecular speed of O_3 and D_g is its gas-phase molecular diffusion coefficient calculated as follows:

$$D_g = \frac{9.45 \times 10^{17} \times \sqrt{T\left(3.47 \times 10^{-2} + \frac{1}{M}\right)}}{\rho_{air}} \quad (A5)$$

where T is the ambient air temperature, ρ_{air} is the air density, and M the molar mass of O_3. γ is the reaction probability calculated following Jacob (Jacob, 2000) and Shao et al. (Shao et al., 2019).

$$\gamma = \left(\frac{1}{\alpha} + \frac{\upsilon}{4HRT\sqrt{D_a K}} \frac{1}{f_r} \right) \quad (A6)$$

280   where α is the mass accommodation coefficient, Da is the aqueous-phase molecular diffusion coefficient of O3, H is the effective Henry's law constant of O_3 (Sander, 2015), R is the ideal gas constant, f_r is the reacto-diffusive correction term (Shao et al., 2019), and K is the pseudo-first order reaction rate constant between S(IV) and O_3 in the aqueous phase (Seinfeld and Pandis, 2006).

5. References

Abdelkader, M., Metzger, S., Mamouri, R. E., Astitha, M., Barrie, L., Levin, Z., and Lelieveld, J.: Dust-air pollution dynamics over the eastern Mediterranean, Atmospheric Chemistry and Physics, 15, 9173-9189, 10.5194/acp-15-9173-2015, 2015.

Akagi, S. K., Yokelson, R. J., Wiedinmyer, C., Alvarado, M. J., Reid, J. S., Karl, T., Crounse, J. D., and Wennberg, P. O.: Emission factors for open and domestic biomass burning for use in atmospheric models, Atmospheric Chemistry and Physics, 11, 4039-4072, 10.5194/acp-11-4039-2011, 2011.

Andreae, M. O., Talbot, R. W., Andreae, T. W., and Harriss, R. C.: Formic and acetic-acid over the central Amazon region, Brazil. 1. dry season, Journal of Geophysical Research-Atmospheres, 93, 1616-1624, 10.1029/JD093iD02p01616, 1988.

Bacer, S., Sullivan, S. C., Karydis, V. A., Barahona, D., Kramer, M., Nenes, A., Tost, H., Tsimpidi, A. P., Lelieveld, J., and Pozzer, A.: Implementation of a comprehensive ice crystal formation parameterization for cirrus and mixed-phase clouds in the EMAC model (based on MESSy 2.53), Geoscientific Model Development, 11, 4021-4041, 10.5194/gmd-11-4021-2018, 2018.

Behera, S. N., Betha, R., Liu, P., and Balasubramanian, R.: A study of diurnal variations of PM2.5 acidity and related chemical species using a new thermodynamic equilibrium model, Science of The Total Environment, 452-453, 286-295, https://doi.org/10.1016/j.scitotenv.2013.02.062, 2013.

Bouwman, A. F., Lee, D. S., Asman, W. A. H., Dentener, F. J., VanderHoek, K. W., and Olivier, J. G. J.: A global high-resolution emission inventory for ammonia, Global Biogeochemical Cycles, 11, 561-587, 10.1029/97gb02266, 1997.

Cheng, Y. F., Zheng, G. J., Wei, C., Mu, Q., Zheng, B., Wang, Z. B., Gao, M., Zhang, Q., He, K. B., Carmichael, G., Poschl, U., and Su, H.: Reactive nitrogen chemistry in aerosol water as a source of sulfate during haze events in China, Science Advances, 2, 10.1126/sciadv.1601530, 2016.

Clegg, S. L., Brimblecombe, P., and Wexler, A. S.: Thermodynamic model of the system H+-NH4+-Na+-SO42--NB3--Cl--H2O at 298.15 K, J. Phys. Chem. A, 102, 2155-2171, 10.1021/jp973043j, 1998.

Atmospheric
Chemistry
and Physics
Discussions

Dall'Osto, M., Airs, R. L., Beale, R., Cree, C., Fitzsimons, M. F., Beddows, D., Harrison, R. M., Ceburnis, D., O'Dowd, C.,
    Rinaldi, M., Paglione, M., Nenes, A., Decesari, S., and Simó, R.: Simultaneous Detection of Alkylamines in the Surface
310   Ocean and Atmosphere of the Antarctic Sympagic Environment, ACS Earth and Space Chemistry, 3, 854-862,
    10.1021/acsearthspacechem.9b00028, 2019.

Dentener, F., Kinne, S., Bond, T., Boucher, O., Cofala, J., Generoso, S., Ginoux, P., Gong, S., Hoelzemann, J. J., Ito, A.,
    Marelli, L., Penner, J. E., Putaud, J. P., Textor, C., Schulz, M., van der Werf, G. R., and Wilson, J.: Emissions of primary
    aerosol and precursor gases in the years 2000 and 1750 prescribed data-sets for AeroCom, Atmos. Chem. Phys., 6, 4321-
315   4344, 2006.

Falkovich, A. H., Graber, E. R., Schkolnik, G., Rudich, Y., Maenhaut, W., and Artaxo, P.: Low molecular weight organic
    acids in aerosol particles from Rondonia, Brazil, during the biomass-burning, transition and wet periods, Atmospheric
    Chemistry and Physics, 5, 781-797, 10.5194/acp-5-781-2005, 2005.

Fang, T., Guo, H. Y., Zeng, L. H., Verma, V., Nenes, A., and Weber, R. J.: Highly Acidic Ambient Particles, Soluble
320   Metals, and Oxidative Potential: A Link between Sulfate and Aerosol Toxicity, Environmental Science & Technology,
    51, 2611-2620, 10.1021/acs.est.6b06151, 2017.

Fountoukis, C., and Nenes, A.: ISORROPIA II: a computationally efficient thermodynamic equilibrium model for K^+-Ca^{2+}-
    Mg^{2+}-NH_4^+-Na^+-SO_4^{2-}-NO_3^--Cl^--H_2O aerosols, Atmospheric Chemistry and Physics, 7, 4639-4659, 2007.

Friese,   E.,   and   Ebel,   A.:   Temperature   Dependent   Thermodynamic   Model   of   the   System
325   H+−NH4+−Na+−SO42−−NO3−−Cl−−H2O,   The   Journal   of   Physical   Chemistry   A,   114,   11595-11631,
    10.1021/jp101041j, 2010.

Grewe, V., Brunner, D., Dameris, M., Grenfell, J. L., Hein, R., Shindell, D., and Staehelin, J.: Origin and variability of upper
    tropospheric nitrogen oxides and ozone at northern mid-latitudes, Atmospheric Environment, 35, 3421-3433,
    10.1016/s1352-2310(01)00134-0, 2001.

330 Guo, H., Xu, L., Bougiatioti, A., Cerully, K. M., Capps, S. L., Hite, J. R., Carlton, A. G., Lee, S. H., Bergin, M. H., Ng, N.
    L., Nenes, A., and Weber, R. J.: Fine-particle water and pH in the southeastern United States, Atmospheric Chemistry
    and Physics, 15, 5211-5228, 10.5194/acp-15-5211-2015, 2015.

Guo, H., Sullivan, A. P., Campuzano-Jost, P., Schroder, J. C., Lopez-Hilfiker, F. D., Dibb, J. E., Jimenez, J. L., Thornton, J.
    A., Brown, S. S., Nenes, A., and Weber, R. J.: Fine particle pH and the partitioning of nitric acid during winter in the
335   northeastern United States, Journal of Geophysical Research-Atmospheres, 121, 10355-10376, 10.1002/2016jd025311,
    2016.

Guo, H., Otjes, R., Schlag, P., Kiendler-Scharr, A., Nenes, A., and Weber, R. J.: Effectiveness of ammonia reduction on
    control of fine particle nitrate, Atmospheric Chemistry and Physics, 18, 12241-12256, 10.5194/acp-18-12241-2018,
    2018.

340 Guo, H. Y., Liu, J. M., Froyd, K. D., Roberts, J. M., Veres, P. R., Hayes, P. L., Jimenez, J. L., Nenes, A., and Weber, R. J.:
    Fine particle pH and gas-particle phase partitioning of inorganic species in Pasadena, California, during the 2010 CalNex
    campaign, Atmospheric Chemistry and Physics, 17, 5703-5719, 10.5194/acp-17-5703-2017, 2017.

Hennigan, C. J., Izumi, J., Sullivan, A. P., Weber, R. J., and Nenes, A.: A critical evaluation of proxy methods used to
    estimate the acidity of atmospheric particles, Atmospheric Chemistry and Physics, 15, 2775-2790, 10.5194/acp-15-2775-
345   2015, 2015.

Jacob, D. J.: Heterogeneous chemistry and tropospheric ozone, Atmospheric Environment, 34, 2131-2159, 10.1016/s1352-
    2310(99)00462-8, 2000.

Jensen, J.: On the convex functions and inequalities between mean values, Acta Mathematica, 30, 175-193,
    10.1007/bf02418571, 1906.

350 Jia, S., Wang, X., Zhang, Q., Sarkar, S., Wu, L., Huang, M., Zhang, J., and Yang, L.: Technical note: Comparison and
    interconversion of pH based on different standard states for aerosol acidity characterization, Atmos. Chem. Phys., 18,
    11125-11133, 10.5194/acp-18-11125-2018, 2018.

Jickells, T. D., An, Z. S., Andersen, K. K., Baker, A. R., Bergametti, G., Brooks, N., Cao, J. J., Boyd, P. W., Duce, R. A.,
    Hunter, K. A., Kawahata, H., Kubilay, N., laRoche, J., Liss, P. S., Mahowald, N., Prospero, J. M., Ridgwell, A. J., Tegen,
355   I., and Torres, R.: Global iron connections between desert dust, ocean biogeochemistry, and climate, Science, 308, 67-71,
    10.1126/science.1105959, 2005.

Jöckel, P., Tost, H., Pozzer, A., Bruehl, C., Buchholz, J., Ganzeveld, L., Hoor, P., Kerkweg, A., Lawrence, M. G., Sander, R., Steil, B., Stiller, G., Tanarhte, M., Taraborrelli, D., Van Aardenne, J., and Lelieveld, J.: The atmospheric chemistry general circulation model ECHAM5/MESSy1: consistent simulation of ozone from the surface to the mesosphere,
360   Atmos. Chem. Phys., 6, 5067-5104, 2006.

Jöckel, P., Kerkweg, A., Pozzer, A., Sander, R., Tost, H., Riede, H., Baumgaertner, A., Gromov, S., and Kern, B.: Development cycle 2 of the Modular Earth Submodel System (MESSy2), Geoscientific Model Development, 3, 717-752, 2010.

Karydis, V. A., Tsimpidi, A. P., Pozzer, A., Astitha, M., and Lelieveld, J.: Effects of mineral dust on global atmospheric
365   nitrate concentrations, Atmos. Chem. Phys., 16, 1491-1509, 10.5194/acp-16-1491-2016, 2016.

Karydis, V. A., Tsimpidi, A. P., Bacer, S., Pozzer, A., Nenes, A., and Lelieveld, J.: Global impact of mineral dust on cloud droplet number concentration, Atmospheric Chemistry and Physics, 17, 5601-5621, 10.5194/acp-17-5601-2017, 2017.

Kerkweg, A., Buchholz, J., Ganzeveld, L., Pozzer, A., Tost, H., and Jöckel, P.: Technical Note: An implementation of the dry removal processes DRY DEPosition and SEDImentation in the Modular Earth Submodel System (MESSy), Atmos.
370   Chem. Phys., 6, 4617-4632, 2006.

Klingmuller, K., Metzger, S., Abdelkader, M., Karydis, V. A., Stenchikov, G. L., Pozzer, A., and Lelieveld, J.: Revised mineral dust emissions in the atmospheric chemistry-climate model EMAC (MESSy 2.52 DU_Astitha1 KKDU2017 patch), Geoscientific Model Development, 11, 989-1008, 10.5194/gmd-11-989-2018, 2018.

Klingmuller, K., Lelieveld, J., Karydis, V. A., and Stenchikov, G. L.: Direct radiative effect of dust-pollution interactions,
375   Atmospheric Chemistry and Physics, 19, 7397-7408, 10.5194/acp-19-7397-2019, 2019.

Klingmüller, K., Karydis, V. A., Bacer, S., Stenchikov, G. L., and Lelieveld, J.: Weaker cooling by aerosols due to dust-pollution interactions, Atmos. Chem. Phys. Discuss., 2020, 1-19, 10.5194/acp-2020-531, 2020.

Lawal, A. S., Guan, X. B., Liu, C., Henneman, L. R. F., Vasilakos, P., Bhogineni, V., Weber, R. J., Nenes, A., and Russell, A. G.: Linked Response of Aerosol Acidity and Ammonia to SO2 and NOx Emissions Reductions in the United States,
380   Environmental Science & Technology, 52, 9861-9873, 10.1021/acs.est.8b00711, 2018.

Lelieveld, J., Evans, J. S., Fnais, M., Giannadaki, D., and Pozzer, A.: The contribution of outdoor air pollution sources to premature mortality on a global scale, Nature, 525, 367-371, 10.1038/nature15371, 2015.

Leygraf, C., Wallinder, I. O., Tidblad, J., and Graedel, T.: Atmospheric Corrosion, John Wiley & Sons, 2016.

Li, C., McLinden, C., Fioletov, V., Krotkov, N., Carn, S., Joiner, J., Streets, D., He, H., Ren, X., Li, Z., and Dickerson, R. R.:
385   India Is Overtaking China as the World's Largest Emitter of Anthropogenic Sulfur Dioxide, Scientific Reports, 7, 14304, 10.1038/s41598-017-14639-8, 2017.

Lohmann, U., and Ferrachat, S.: Impact of parametric uncertainties on the present-day climate and on the anthropogenic aerosol effect, Atmos. Chem. Phys., 10, 11373-11383, 10.5194/acp-10-11373-2010, 2010.

Marais, E. A., Jacob, D. J., Jimenez, J. L., Campuzano-Jost, P., Day, D. A., Hu, W., Krechmer, J., Zhu, L., Kim, P. S.,
390   Miller, C. C., Fisher, J. A., Travis, K., Yu, K., Hanisco, T. F., Wolfe, G. M., Arkinson, H. L., Pye, H. O. T., Froyd, K. D., Liao, J., and McNeill, V. F.: Aqueous-phase mechanism for secondary organic aerosol formation from isoprene: application to the southeast United States and co-benefit of SO2 emission controls, Atmospheric Chemistry and Physics, 16, 1603-1618, 10.5194/acp-16-1603-2016, 2016.

Masiol, M., Squizzato, S., Formenton, G., Khan, M. B., Hopke, P. K., Nenes, A., Pandis, S. N., Tositti, L., Benetello, F.,
395   Visin, F., and Pavoni, B.: Hybrid multiple-site mass closure and source apportionment of PM2.5 and aerosol acidity at major cities in the Po Valley, Science of The Total Environment, 704, 135287, https://doi.org/10.1016/j.scitotenv.2019.135287, 2020.

McCormick, M. P., Thomason, L. W., and Trepte, C. R.: ATMOSPHERIC EFFECTS OF THE MT-PINATUBO ERUPTION, Nature, 373, 399-404, 10.1038/373399a0, 1995.

400   Metzger, S., Mihalopoulos, N., and Lelieveld, J.: Importance of mineral cations and organics in gas-aerosol partitioning of reactive nitrogen compounds: case study based on MINOS results, Atmospheric Chemistry and Physics, 6, 2549-2567, 10.5194/acp-6-2549-2006, 2006.

Nah, T., Guo, H., Sullivan, A. P., Chen, Y., Tanner, D. J., Nenes, A., Russell, A., Ng, N. L., Huey, L. G., and Weber, R. J.: Characterization of aerosol composition, aerosol acidity, and organic acid partitioning at an agriculturally intensive rural
405   southeastern US site, Atmos. Chem. Phys., 18, 11471-11491, 10.5194/acp-18-11471-2018, 2018.

Nenes, A., Pandis, S. N., Weber, R. J., and Russell, A.: Aerosol pH and liquid water content determine when particulate matter is sensitive to ammonia and nitrate availability, Atmospheric Chemistry and Physics, 20, 3249-3258, 10.5194/acp-20-3249-2020, 2020.

410 Oakes, M., Ingall, E. D., Lai, B., Shafer, M. M., Hays, M. D., Liu, Z. G., Russell, A. G., and Weber, R. J.: Iron Solubility Related to Particle Sulfur Content in Source Emission and Ambient Fine Particles, Environmental Science & Technology, 46, 6637-6644, 10.1021/es300701c, 2012.

Park, M., Joo, H. S., Lee, K., Jang, M., Kim, S. D., Kim, I., Borlaza, L. J. S., Lim, H., Shin, H., Chung, K. H., Choi, Y.-H., Park, S. G., Bae, M.-S., Lee, J., Song, H., and Park, K.: Differential toxicities of fine particulate matters from various sources, Scientific Reports, 8, 17007, 10.1038/s41598-018-35398-0, 2018.

415 Pathak, R. K., Yao, X. H., and Chan, C. K.: Sampling artifacts of acidity and ionic species in PM2.5, Environmental Science & Technology, 38, 254-259, 10.1021/es0342244, 2004.

Pathak, R. K., Wu, W. S., and Wang, T.: Summertime PM$_{2.5}$ ionic species in four major cities of China: nitrate formation in an ammonia-deficient atmosphere, Atmos. Chem. Phys., 9, 1711-1722, 10.5194/acp-9-1711-2009, 2009.

Petters, M. D., and Kreidenweis, S. M.: A single parameter representation of hygroscopic growth and cloud condensation
420 nucleus activity, Atmospheric Chemistry and Physics, 7, 1961-1971, 2007.

Pozzer, A., Joeckel, P. J., Sander, R., Williams, J., Ganzeveld, L., and Lelieveld, J.: Technical note: the MESSy-submodel AIRSEA calculating the air-sea exchange of chemical species, Atmos. Chem. Phys., 6, 5435-5444, 2006.

Pozzer, A., Jockel, P., and Van Aardenne, J.: The influence of the vertical distribution of emissions on tropospheric chemistry, Atmospheric Chemistry and Physics, 9, 9417-9432, 2009.

425 Pozzer, A., de Meij, A., Pringle, K. J., Tost, H., Doering, U. M., van Aardenne, J., and Lelieveld, J.: Distributions and regional budgets of aerosols and their precursors simulated with the EMAC chemistry-climate model, Atmos. Chem. Phys.. 12, 961-987, 2012.

Pozzer, A., Tsimpidi, A. P., Karydis, V. A., de Meij, A., and Lelieveld, J.: Impact of agricultural emission reductions on fine-particulate matter and public health, Atmospheric Chemistry and Physics, 17, 12813-12826, 10.5194/acp-17-12813-
430 2017, 2017.

Pringle, K. J., Tost, H., Message, S., Steil, B., Giannadaki, D., Nenes, A., Fountoukis, C., Stier, P., Vignati, E., and Leieved, J.: Description and evaluation of GMXe: a new aerosol submodel for global simulations (v1), Geoscientific Model Development, 3, 391-412, 2010.

Pye, H. O. T., Nenes, A., Alexander, B., Ault, A. P., Barth, M. C., Clegg, S. L., Collett, J. L., Fahey, K. M., Hennigan, C. J.,
435 Herrmann, H., Kanakidou, M., Kelly, J. T., Ku, I. T., McNeill, V. F., Riemer, N., Schaefer, T., Shi, G. L., Tilgner, A., Walker, J. T., Wang, T., Weber, R., Xing, J., Zaveri, R. A., and Zuend, A.: The acidity of atmospheric particles and clouds, Atmospheric Chemistry and Physics, 20, 4809-4888, 10.5194/acp-20-4809-2020, 2020.

Raizenne, M., Neas, L. M., Damokosh, A. I., Dockery, D. W., Spengler, J. D., Koutrakis, P., Ware, J. H., and Speizer, F. E.: Health effects of acid aerosols on North American children: Pulmonary function, Environmental Health Perspectives,
440 104, 506-514, 10.2307/3432991, 1996.

Roeckner, E., Brokopf, R., Esch, M., Giorgetta, M., Hagemann, S., Kornblueh, L., Manzini, E., Schlese, U., and Schulzweida, U.: Sensitivity of simulated climate to horizontal and vertical resolution in the ECHAM5 atmosphere model, Journal of Climate, 19, 3771-3791, 10.1175/jcli3824.1, 2006.

Saiz-Lopez, A., and von Glasow, R.: Reactive halogen chemistry in the troposphere, Chemical Society Reviews, 41, 6448-
445 6472, 10.1039/c2cs35208g, 2012.

Sander, R.: Compilation of Henry's law constants (version 4.0) for water as solvent, Atmos. Chem. Phys., 15, 4399-4981, 10.5194/acp-15-4399-2015, 2015.

Sander, R., Baumgaertner, A., Cabrera-Perez, D., Frank, F., Gromov, S., Grooss, J. U., Harder, H., Huijnen, V., Jockel, P., Karydis, V. A., Niemeyer, K. E., Pozzer, A., Hella, R. B., Schultz, M. G., Taraborrelli, D., and Tauer, S.: The community
450 atmospheric chemistry box model CAABA/MECCA-4.0, Geoscientific Model Development, 12, 1365-1385, 10.5194/gmd-12-1365-2019, 2019.

Seinfeld, J. H., and Pandis, S. N.: Atmospheric Chemistry and Physics: From Air Pollution to Climate Change, Second ed., John Wiley & Sons, Inc., Hoboken, New Jersey, 2006.

Shao, J., Chen, Q., Wang, Y., Lu, X., He, P., Sun, Y., Shah, V., Martin, R. V., Philip, S., Song, S., Zhao, Y., Xie, Z., Zhang,
455 L., and Alexander, B.: Heterogeneous sulfate aerosol formation mechanisms during wintertime Chinese haze events: air

quality model assessment using observations of sulfate oxygen isotopes in Beijing, Atmos. Chem. Phys., 19, 6107-6123, 10.5194/acp-19-6107-2019, 2019.

Shi, G., Xu, J., Peng, X., Xiao, Z., Chen, K., Tian, Y., Guan, X., Feng, Y., Yu, H., Nenes, A., and Russell, A. G.: pH of Aerosols in a Polluted Atmosphere: Source Contributions to Highly Acidic Aerosol, Environmental Science & Technology, 51, 4289-4296, 10.1021/acs.est.6b05736, 2017.

Song, S., Gao, M., Xu, W., Shao, J., Shi, G., Wang, S., Wang, Y., Sun, Y., and McElroy, M. B.: Fine-particle pH for Beijing winter haze as inferred from different thermodynamic equilibrium models, Atmos. Chem. Phys., 18, 7423-7438, 10.5194/acp-18-7423-2018, 2018.

Squizzato, S., Masiol, M., Brunelli, A., Pistollato, S., Tarabotti, E., Rampazzo, G., and Pavoni, B.: Factors determining the formation of secondary inorganic aerosol: a case study in the Po Valley (Italy), Atmos. Chem. Phys., 13, 1927-1939, 10.5194/acp-13-1927-2013, 2013.

Sullivan, R. C., Moore, M. J. K., Petters, M. D., Kreidenweis, S. M., Roberts, G. C., and Prather, K. A.: Effect of chemical mixing state on the hygroscopicity and cloud nucleation properties of calcium mineral dust particles, Atmospheric Chemistry and Physics, 9, 3303-3316, 2009.

Surratt, J. D., Chan, A. W. H., Eddingsaas, N. C., Chan, M. N., Loza, C. L., Kwan, A. J., Hersey, S. P., Flagan, R. C., Wennberg, P. O., and Seinfeld, J. H.: Reactive intermediates revealed in secondary organic aerosol formation from isoprene, Proceedings of the National Academy of Sciences of the United States of America, 107, 6640-6645, 10.1073/pnas.0911114107, 2010.

Tan, T., Hu, M., Li, M., Guo, Q., Wu, Y., Fang, X., Gu, F., Wang, Y., and Wu, Z.: New insight into PM2.5 pollution patterns in Beijing based on one-year measurement of chemical compositions, Science of The Total Environment, 621, 734-743, https://doi.org/10.1016/j.scitotenv.2017.11.208, 2018.

Tost, H., Jockel, P. J., Kerkweg, A., Sander, R., and Lelieveld, J.: Technical note: A new comprehensive SCAVenging submodel for global atmospheric chemistry modelling, Atmos. Chem. Phys., 6, 565-574, 2006.

Tsimpidi, A. P., Karydis, V. A., Pozzer, A., Pandis, S. N., and Lelieveld, J.: ORACLE (v1.0): module to simulate the organic aerosol composition and evolution in the atmosphere, Geoscientific Model Development, 7, 3153-3172, 10.5194/gmd-7-3153-2014, 2014.

Tsimpidi, A. P., Karydis, V. A., Pandis, S. N., and Lelieveld, J.: Global combustion sources of organic aerosols: model comparison with 84 AMS factor-analysis data sets, Atmos. Chem. Phys., 16, 8939-8962, 10.5194/acp-16-8939-2016, 2016.

Tsimpidi, A. P., Karydis, V. A., Pozzer, A., Pandis, S. N., and Lelieveld, J.: ORACLE 2-D (v2.0): an efficient module to compute the volatility and oxygen content of organic aerosol with a global chemistry-climate model, Geoscientific Model Development, 11, 3369-3389, 10.5194/gmd-11-3369-2018, 2018.

van Vuuren, D. P., Edmonds, J., Kainuma, M., Riahi, K., Thomson, A., Hibbard, K., Hurtt, G. C., Kram, T., Krey, V., Lamarque, J. F., Masui, T., Meinshausen, M., Nakicenovic, N., Smith, S. J., and Rose, S. K.: The representative concentration pathways: an overview, Climatic Change, 109, 5-31, 10.1007/s10584-011-0148-z, 2011.

Vieira-Filho, M., Pedrotti, J. J., and Fornaro, A.: Water-soluble ions species of size-resolved aerosols: Implications for the atmospheric acidity in São Paulo megacity, Brazil, Atmospheric Research, 181, 281-287, https://doi.org/10.1016/j.atmosres.2016.07.006, 2016.

Vignati, E., Wilson, J., and Stier, P.: M7: An efficient size-resolved aerosol microphysics module for large-scale aerosol transport models, J. Geophys. Res.-Atmos., 109, doi: 10.1029/2003jd004485, 2004.

Wang, H., Ding, J., Xu, J., Wen, J., Han, J., Wang, K., Shi, G., Feng, Y., Ivey, C. E., Wang, Y., Nenes, A., Zhao, Q., and Russell, A. G.: Aerosols in an arid environment: The role of aerosol water content, particulate acidity, precursors, and relative humidity on secondary inorganic aerosols, Science of The Total Environment, 646, 564-572, https://doi.org/10.1016/j.scitotenv.2018.07.321, 2019a.

Wang, Y., Li, W., Gao, W., Liu, Z., Tian, S., Shen, R., Ji, D., Wang, S., Wang, L., Tang, G., Song, T., Cheng, M., Wang, G., Gong, Z., Hao, J., and Zhang, Y.: Trends in particulate matter and its chemical compositions in China from 2013–2017, Science China Earth Sciences, 62, 1857-1871, 10.1007/s11430-018-9373-1, 2019b.

Weber, R. J., Guo, H. Y., Russell, A. G., and Nenes, A.: High aerosol acidity despite declining atmospheric sulfate concentrations over the past 15 years, Nature Geoscience, 9, 282-285, 10.1038/ngeo2665, 2016.

Atmospheric
Chemistry
and Physics
Discussions

505   Xu, L., Guo, H. Y., Boyd, C. M., Klein, M., Bougiatioti, A., Cerully, K. M., Hite, J. R., Isaacman-VanWertz, G., Kreisberg, N. M., Knote, C., Olson, K., Koss, A., Goldstein, A. H., Hering, S. V., de Gouw, J., Baumann, K., Lee, S. H., Nenes, A., Weber, R. J., and Ng, N. L.: Effects of anthropogenic emissions on aerosol formation from isoprene and monoterpenes in the southeastern United States, Proceedings of the National Academy of Sciences of the United States of America, 112, 37-42, 10.1073/pnas.1417609112, 2015.

510   Xue, J., Lau, A. K. H., and Yu, J. Z.: A study of acidity on PM2.5 in Hong Kong using online ionic chemical composition measurements, Atmospheric Environment, 45, 7081-7088, https://doi.org/10.1016/j.atmosenv.2011.09.040, 2011.

Yao, X., Ling, T. Y., Fang, M., and Chan, C. K.: Size dependence of in situ pH in submicron atmospheric particles in Hong Kong, Atmospheric Environment, 41, 382-393, https://doi.org/10.1016/j.atmosenv.2006.07.037, 2007.

Yienger, J. J., and Levy, H.: Empirical-model of global soil-biogenic NOx emissions, Journal of Geophysical Research-
515   Atmospheres, 100, 11447-11464, 10.1029/95jd00370, 1995.

Zakoura, M., Kakavas, S., Nenes, A., and Pandis, S. N.: Size-resolved aerosol pH over Europe during summer, Atmos. Chem. Phys. Discuss., 2020, 1-24, 10.5194/acp-2019-1146, 2020.

Zheng, G., Su, H., Wang, S., Andreae, M. O., Pöschl, U., and Cheng, Y.: Multiphase buffer theory explains contrasts in atmospheric aerosol acidity, Science, 369, 1374-1377, 10.1126/science.aba3719, 2020.

520

Author contributions: V.A.K. and J.L. planned the research, V.A.K., A.P.T. and A.P. performed the model calculations, V.A.K., A.P., and J.L. analyzed the results, V.A.K. and J.L. wrote the paper. All authors contributed to the manuscript.;

Competing interests: Authors declare no competing interests. **Code/Data availability:** Data and related material can be
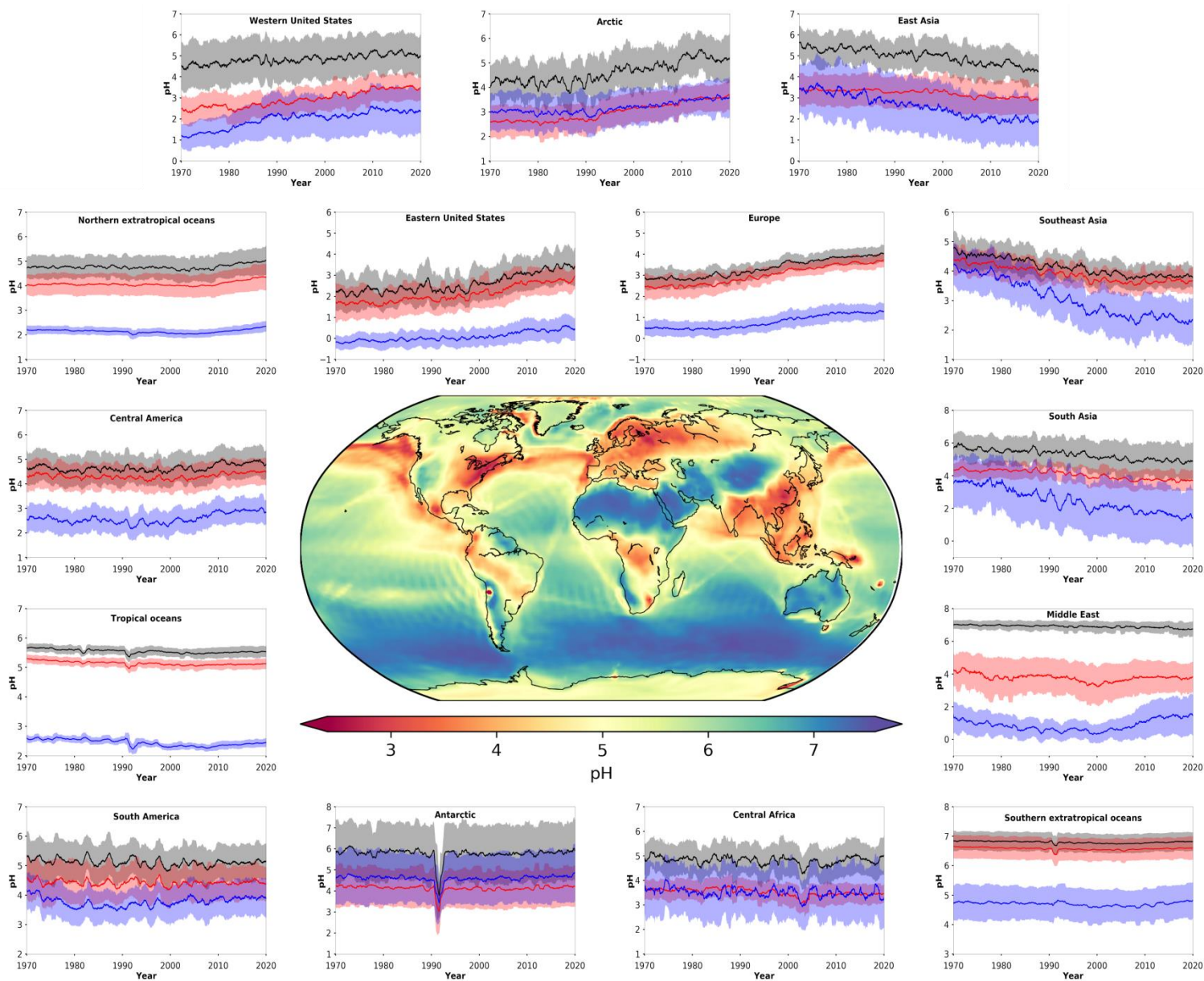525   obtained from V.A.K. (v.karydis@fz-juelich.de) upon request.

Figure 1: Mean, near-surface fine aerosol pH during the period 2010-2015 (central panel). Surrounding panels show the temporal pH evolution at locations defined in Table 1. Black lines represent the reference simulation. Red and blue lines show the sensitivity simulations in which crustal particle and NH$_3$ emissions are removed, respectively. Ranges represent the 1σ standard deviation. The anomaly in 1991/2 is related to the Mt Pinatubo eruption.
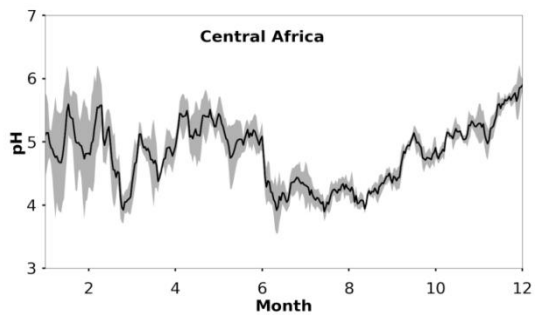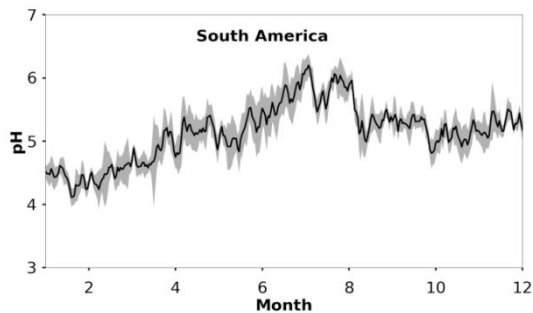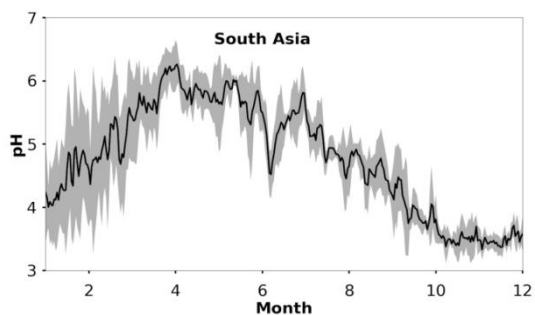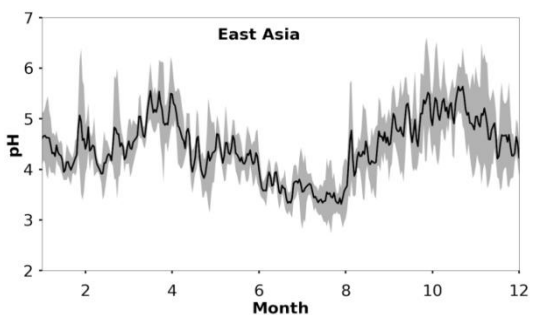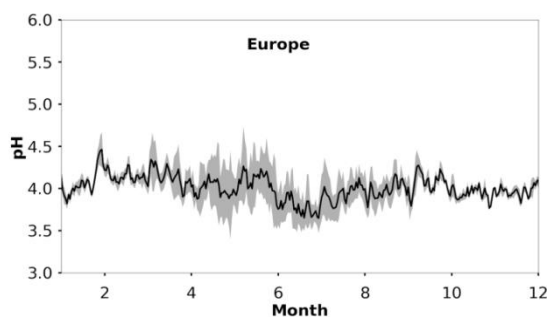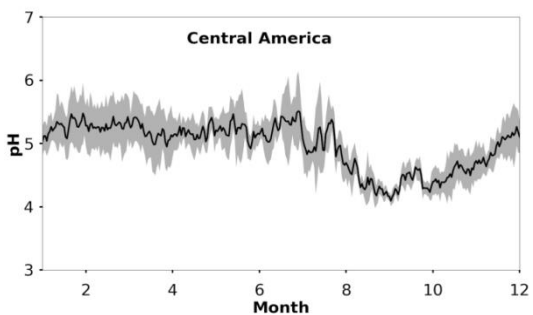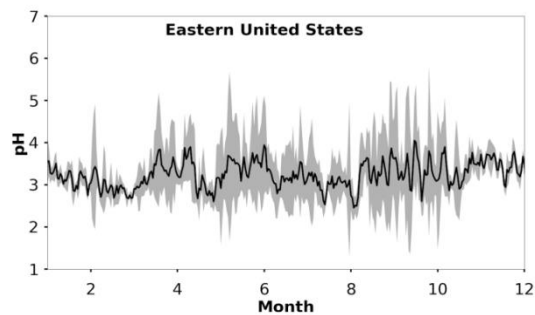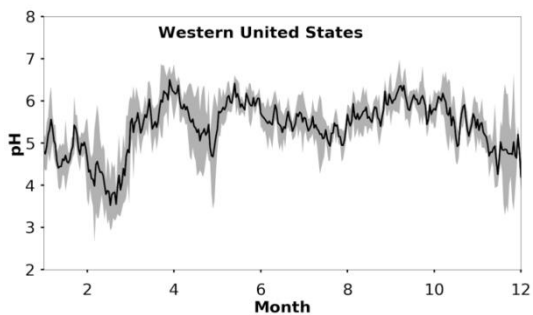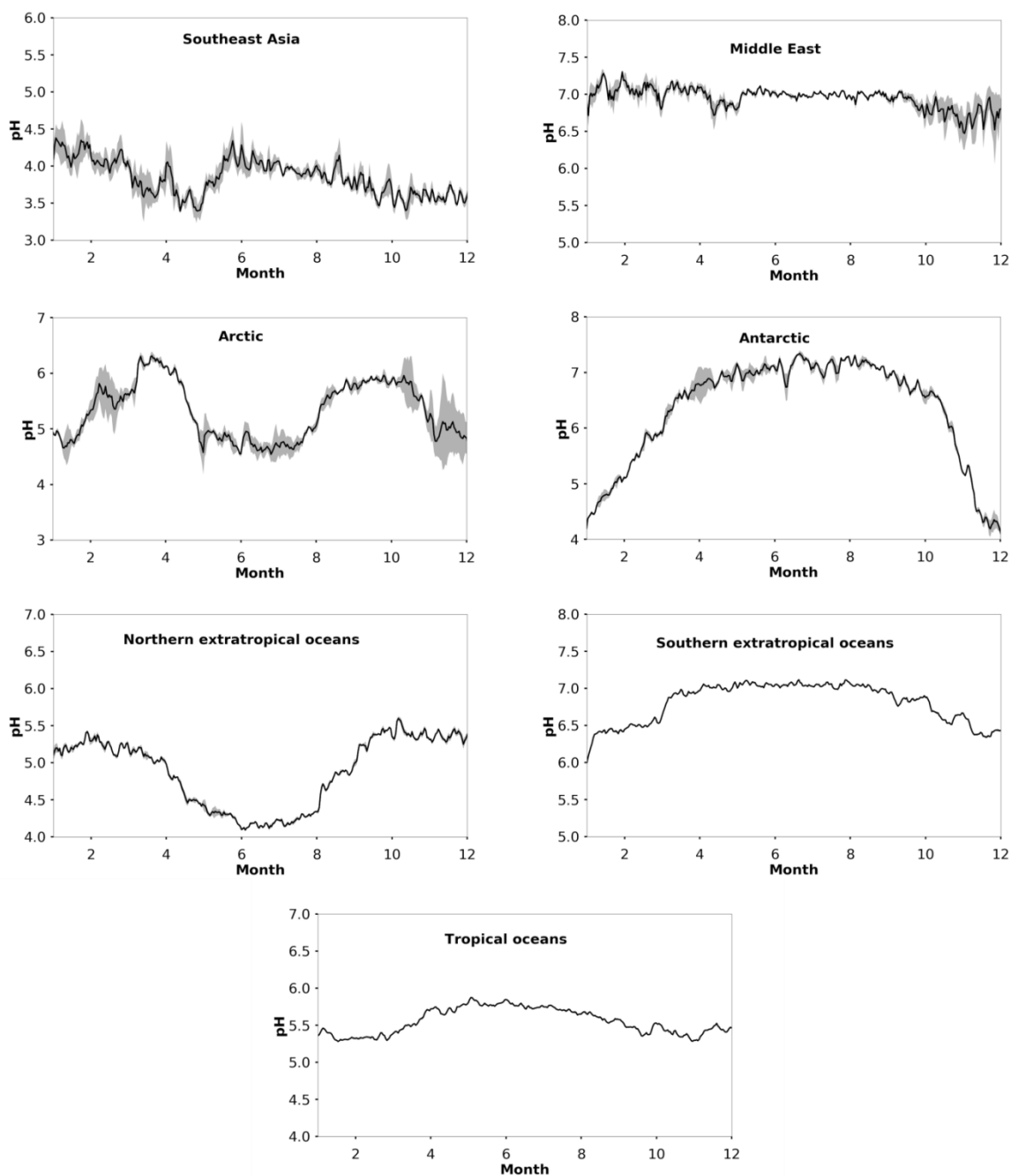
Figure 2: Average seasonal cycle of modelled pH during the period 2010-2015 at locations defined in Table 1. Ranges represent the 1σ standard deviation.
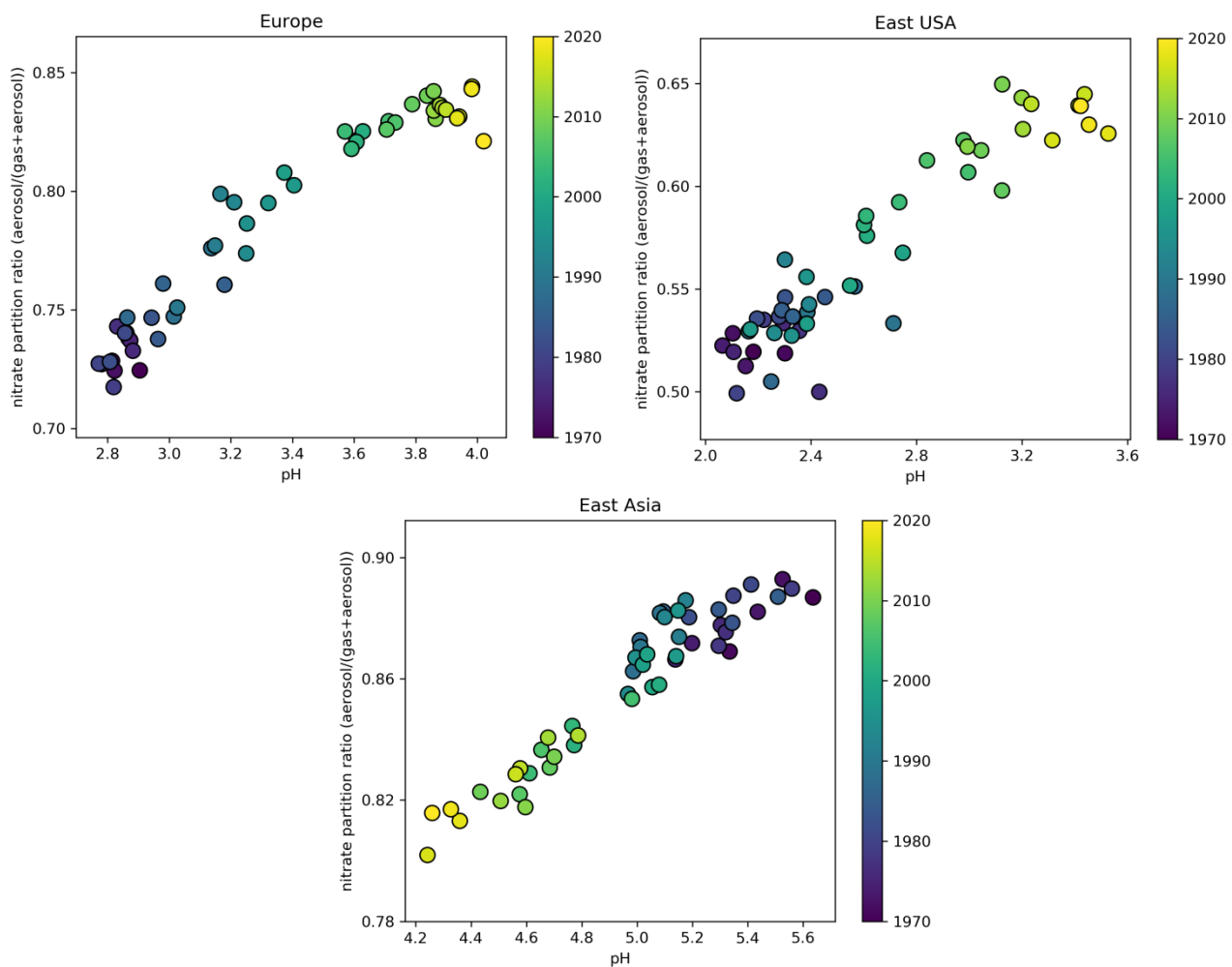
Figure 3: Time evolution of particle phase fraction of total nitrate as a function of pH over Europe (left), the Eastern USA (right) and East Asia (bottom) during the period 1970-2020.
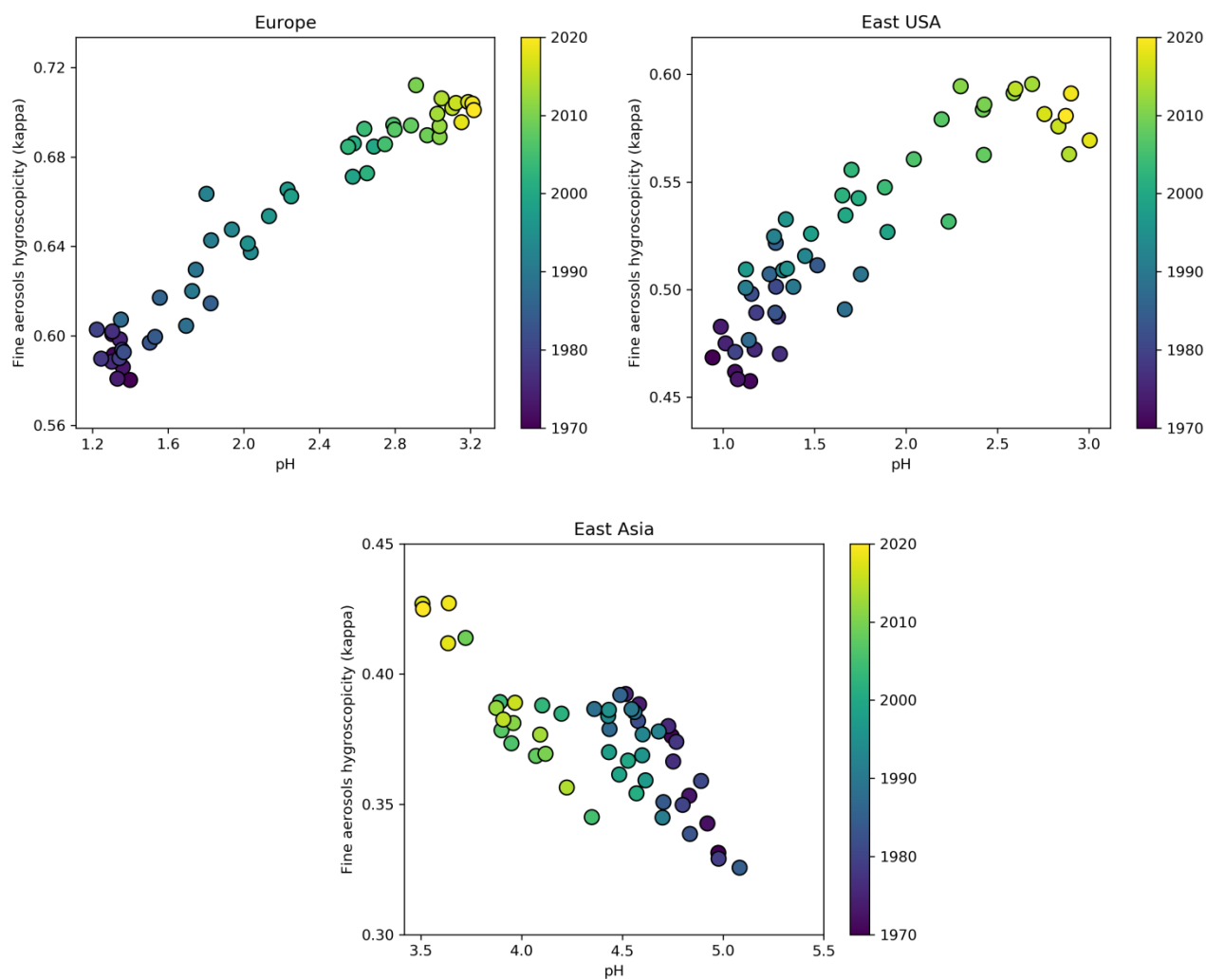
Figure 4: Time evolution of annual average aerosol hygroscopicity (Kappa) as a function of pH over Europe (left), the Eastern USA (right) and East Asia (bottom) during the period 1970-2020 at the lowest cloud-forming level (940 hPa).
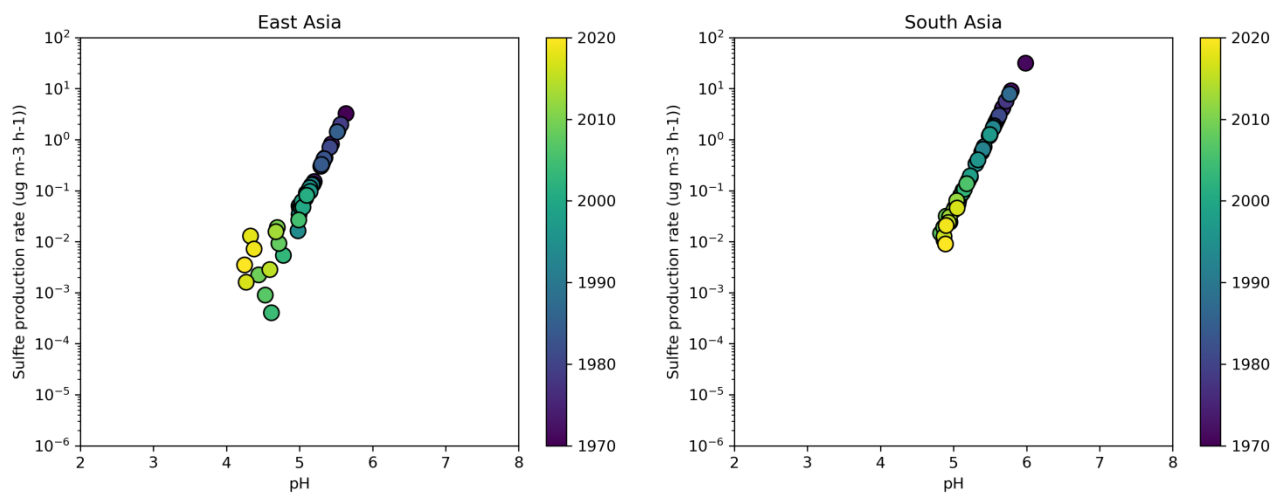
Figure 5: Time evolution of the sulfate production rate on aqueous aerosols from the SO_2+O_3 multiphase chemistry reaction as a function of aerosol pH over East Asia (left) and South Asia (right) during the period 1970-2020.

Atmospheric
Chemistry
and Physics
Discussions

Table 1: Decadal averages of aerosol pH.

Region	Longitude	Latitude	1971-1980	1981-1990	1991-2000	2001-2010	2011-2020
Western USA[1]	90°-70°W	30°-46°N	4.6	4.8	4.8	5.0	5.1
Eastern USA[1]	124°-114°W	30°-52°N	2.2	2.4	2.4	2.9	3.3
Central America[1]	106°-52°W	4°-28°N	4.6	4.6	4.6	4.7	4.9
Europe[1]	12°W-36°E	34°-62°N	2.8	3.0	3.3	3.7	3.9
East Asia[1]	100°-114°E	20°-44°N	5.3	5.2	5.1	4.7	4.5
South Asia[1]	68°-94°E	8°-32°N	5.6	5.5	5.3	5.0	4.9
South America[1]	75°-35°W	30°-0°S	5.2	5.1	5.1	5.1	5.1
Central Africa[1]	10°-40°E	10°S-10°N	4.9	4.8	4.8	4.7	4.9
Southeast Asia[1]	94°-130°E	12°S-20°N	4.5	4.3	4.1	3.9	3.8
Middle East[1]	36°-60°E	12°-34°N	7.0	7.0	6.9	6.9	6.8
Arctic	0°-360°	60°-90°N	4.2	4.2	4.6	4.8	5.2
North extratropics[2]	0°-360°	20°-60°N	4.8	4.8	4.7	4.7	4.9
Tropical oceans[2]	0°-360°	20°S-20°N	5.6	5.6	5.5	5.5	5.5
South extratropics[2]	0°-360°	60°-20°S	6.8	6.8	6.8	6.8	6.8
Antarctic	0°-360°	90°-60°S	5.9	5.9	5.6	5.8	5.8

[1]Only values over land are considered for the calculation of pH

[2]Only values over oceans are considered for the calculation of pH